**Science and Technology Indonesia**
*e*-ISSN:2580-4391 *p*-ISSN:2580-4405
Vol. 5, No. 4, October 2020

Research Paper

# Characteristics of Diurnal Rainfall over Peatland Area of South Sumatra, Indonesia

Puad Maulana Mandailing[1], Wijaya Mardiansyah[2], Muhammad Irfan[2], Arsali[2], Iskhaq Iskandar[2*]

[1] *Graduate School of Physics, University of Sriwijaya, Palembang, South Sumatera, Indonesia*
[2] *Department of Physics, Faculty of Mathematics and Natural Sciences, University of Sriwijaya, Indralaya, Ogan Ilir, South Sumatera, Indonesia*
[*] **Corresponding author**: Iskhaq@mipa.unsri.ac.id

**Abstract**
The peak time of rainfall occurrence over an area has certain characteristics in which the difference in time and intensity of rainfall varies depending on its location and distance from the sea. This variation can be determined based on the phase and amplitude obtained using harmonic analysis. In this study, combined data from in-situ observation, satellite remote sensing and reanalysis were used to analyze spatial and temporal variations of peak rainfall events over peatland area of the South Sumatra Province. The results show that most of the South Sumatra Province has a diurnal peak of rainfall during afternoon ranging from 16.00 to 19.00 Western Indonesian Time. In addition, the results also indicate that the analysis on the in situ data revealed seasonal variation both in amplitude and time of maximum diurnal rainfall, while the reanalysis data only indicated a weak seasonal variation on the amplitude of the diurnal rainfall. Furthermore, spatial analysis shows that the time of maximum diurnal rainfall has spatial variation. Over the ocean, the time of maximum diurnal rainfall occurs during night time/early morning. Over the lowland or coastal area, the time of maximum diurnal rainfall occurs during afternoon, while over the high altitude (mountain) it occurs during late night.

**Keywords**
Diurnal Rainfall, Peatland, SESAME, ECMWF-ERA5

Received: 25 September 2020, Accepted: 8 October 2020
https://doi.org/10.26554/sti.2020.5.4.136-141

## 1. INTRODUCTION

Several studies have been done to evaluate the diurnal variations of rainfall in the tropical region using available observation and satellite remote sensing as well as model output (Wallace, 1975; Murakami (1983); Houze Jr et al. (1981); Dai, 2001; Gray and Jacobson Jr (1977); Mori et al. (2004). The results show that rainfall peak events usually occur in the afternoon/evening over the land areas/islands, while it is observed in the early morning over the areas close to ocean areas such as coastal areas. In particular, Mori et al. (2004) showed a propagation of rainfall peak from the southwestern coastline of Sumatera into the island during day time, while during nighttime it propagates toward the offshore region. In addition, recent study has shown that diurnal rainfall peak events occur in the afternoon over the coastal areas and at midnight over the adjacent sea region (Biasutti et al., 2011).

It has been known that the peatland are in Indonesia, including that in the South Sumatera, is vulnerable to fire during the dry season (Putra (2019)a; Putra et al. (2019)b. It was suggested that the El Niño and/or positive Indian Ocean Dipole provided a favorable condition for peat fires as the rainfall over the Indonesian regions was significantly reduce Putra (2019). In particular, the peat fires associated with those two climate modes were mainly observed in the land cover types of ferns/shrub (Putra et al., 2019).

This study is designed to evaluate characteristics of diurnal rainfall over the peatland area of South Sumatera using available observational (e.g. in-situ and satellite remote sensing) and re-analysis data. Having information on the diurnal rainfall variability will be useful to determine the time and location of cloud seeding for weather modification during the forest/peat fire. The weather medication technique is believed to be effective to reduce severe forest/peat fires during the last two decades associated with extreme drought events.

## 2. EXPERIMENTAL SECTION

### 2.1 Materials

In this study, the in situ rainfall data were collected under the Sensory Data Transmission Service Assisted by Midori Engineering Laboratory (SESAME) project. The project is under the Peatlad Restoration Agency (Badan Restorasi Gambut - BRG) of Indonesia, which designed to monitor the hydrological condi-

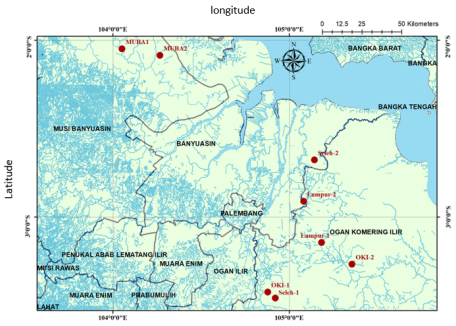


**Figure 1.** The location of study in the peatland of South Sumatera. The red-circle indicated the location of SESAME stations.

tion of peat area in Indonesia. In addition, the reanalysis data obtained from the European Center for Medium-Range Weather Forecast (ECMWF) – ERA5 was also used for comparison as well as spatial analysis. The detailed data description is shown in Table 1. The location of study is shown in Figure 1, while the location of SESAME stations are listed in Table 2.

### 2.2 Methods

In this study, a harmonic analysis is used to evaluate the characteristics of diurnal rainfall variations over the study area. Note that the harmonic analysis provides information on the amplitude (intensity) and phase (time) of the peak in the daily rainfall. The analysis starts with determining the average value of monthly rainfall intensity per unit hour ($Pa$) as follow Angelis et al. (2004),

$$P_a(h) = \frac{\sum_{d=1}^{N} P(h,d)}{N}, \tag{1}$$

where $h$ indicates the specified hour in a day (e.g. 1 – 24), $d$ is the day during which the hourly data used, and $N$ is the total number of day.

The rainfall data can be constructed into a time series as follow,

$$P_a(h) = \bar{P} + \sum_{k} C_k cos\left(\frac{2\pi kh}{n} - \Phi_k\right) + residual, \tag{2}$$

where $\bar{P}$ is the mean of the rainfall data and $k$ is a harmonic number. $C_k$ and $\Phi_k$ are the amplitude and phase for the given harmonic number, respectively. $n$ is the period which is 24 hours for hourly data, and $h$ is the specified hour. Equation (2.2) can be solved as,

$$A_k = \frac{2}{n} + \sum_{h=1}^{n} P_h cos\left(\frac{2\pi kh}{n}\right) \tag{3}$$

$$B_k = \frac{2}{n} + \sum_{h=1}^{n} P_h sin\left(\frac{2\pi kh}{n}\right) \tag{4}$$

The amplitude ($C_k$) and the phase ($\Phi_k$) can be calculated by suing the following equations,

$$C_k = \left[A_k^2 + B_k^2\right]^{\frac{1}{2}}, \tag{5}$$

$$\Phi_k = \begin{cases} tan^{-1}\left(\frac{B_k}{A_k}\right), & A_k > 0 \\ tan^{-1}\left(\frac{B_k}{A_k}\right) \pm \pi, \text{or} \pm 180^o & A_k < 0 \\ \frac{\pi}{2}, \text{or} 90^o & A_k = 0 \end{cases} \tag{6}$$

The accuracy and uncertainty of the ERA5 data were obtained using a contingency table analysis of "yes" or "no" rainfall events Stull et al. (2018). The contingency table can be seen in table 3.

A contingency table (Table 3) has cells for each possible combination of binary model and observation outcomes. “Hit” means the event was successfully model. “Miss” means it occurred but was not model. “False Alarm” means it was a model but did not happen. “Correct Negatif” means that the event was correctly model to not occur.

The bias score B indicates over- or under-prediction of the frequency of event occurrence:

$$B = \frac{hit + Miss}{hit + False\ Alarm} \tag{7}$$

A critical success index CSI (also known as a threat score TS) is:

$$CSI = \frac{hit}{hit + miss + False\ Alarm} \tag{8}$$

## 3. RESULTS AND DISCUSSION

### 3.1 Time of Maximum Diurnal Rainfall (Peak Time)

Before we analyze the diurnal cycle of the in situ rainfall, we first evaluate the completeness of rainfall data recorded by the SESAME stations. Table 3 shows the percentage of available data at each station during the period of observation from January 2017 through December 2019. In this study, we only used the station having a complete dataset in each month.

The diurnal cycle of in situ rainfall in each season, namely the northwest monsoon season (December-January-February/DJF), the first monsoon break season (March-April-May/MAM), the southeast monsoon season (June-July-August/JJA), and the second monsoon break season (September-October-November/SON), is shown in Figure 2. The amplitude and the time of maximum diurnal rainfall clearly show seasonal variations. As it was expected, low amplitude of diurnal rainfall was observed during

**Table 1.** List of data used in the present study

| No | Parameter | Source of data | Type of data | Spatial Resolution | Temporal Resolution | Period |
|---|---|---|---|---|---|---|
| 1 | Precipitation | BRG | In situ | - | Hourly | 2017-2019 |
| 2 | Precipitation | ECMWF-ERA5 | Reanalysis | 0.25 x 0.25 | Hourly | 2017-2019 |

**Table 2.** The location of SESAME stations

| No | Name of Station | Latitude | Longitude |
|---|---|---|---|
| 1 | OKI-1 | -3.4242 $^{o}$S | 104.8785 $^{o}$E |
| 2 | OKI-2 | -3.2670 $^{o}$S | 105.3568 $^{o}$E |
| 3 | MUBA1 | -2.0475 $^{o}$S | 104.0513 $^{o}$E |
| 4 | MUBA2 | -2.0854 $^{o}$S | 104.2674 $^{o}$E |
| 5 | Lumpur-1 | -3.1436 $^{o}$S | 105.1844 $^{o}$E |
| 6 | Lumpur-2 | -2.9107 $^{o}$S | 105.0825 $^{o}$E |
| 7 | Saleh-1 | -3.4584 $^{o}$S | 104.9210 $^{o}$E |
| 8 | Saleh-2 | -2.6769 $^{o}$S | 105.1434 $^{o}$E |

**Table 3.** Contigency table

| | | Actual | |
|---|---|---|---|
| | | Y | N |
| Model | Y | Hit | Miss |
| | N | False Alarm | Correct Negatif |

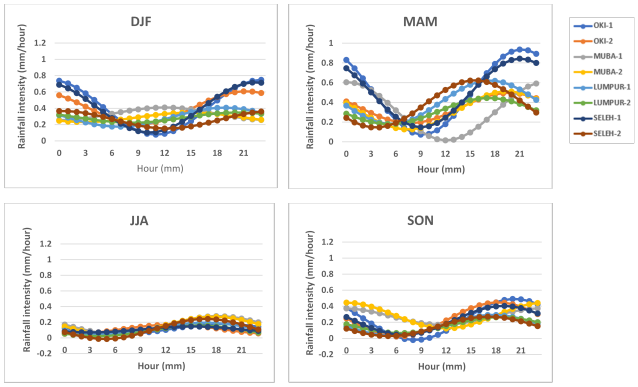


**Figure 2.** Time series of diurnal harmonic of in situ rainfall in each season: DJF season (top-left), MAM season (top-right), JJA season (bottom-left), and SON season (bottom-right).

the dry season in JJA, while the high amplitude of diurnal rainfall was observed during other seasons. During DJF season, the peak time is observed between 11:00 PM all stations except 08:00 (Lumpur-2) and 10:00 (Seleh-1). The time of maximum diurnal rainfall during the MAM season is more confined to the evening (05:00 PM) to early night (11:00 PM). During the dry season in JJA, the time of maximum diurnal rainfall at all stations was observed almost at the same time between 05:00 PM to 11:00 PM. Meanwhile, during the SON season, the time of maximum diurnal rainfall slightly shifted to late evening from 05.00 PM to 11.00 PM. The detailed time of maximum diurnal rainfall at all stations during those four seasons is presented in Table 4.

We found that the time of maximum diurnal rainfall during the dry season (JJA) and the second monsoon break (SON) was observed almost at the same time. Note that the forest fires only occurred during these two seasons with peak fires usually occur in August – October (Putra et al., 2019). By considering the time of maximum diurnal rainfall, we may estimate the time of cloud formation during this dry season. Therefore, the cloud seeding can be organized more effectively weather modification during the dry season.

A similar analysis was conducted for the precipitation data obtained from ECMWF-ERA5. Especially for the ERA5 grid data, the calculation is done by getting the rainfall value that occurs at each observation point that has been determined by ERA5 with a grid resolution of 0.25 degrees. so that each observation point is calculated one by one using the harmonic analysis method. Noted that the precipitation data was generated by spatially averaged the gridded ECMWF-ERA5 data over the SESAME station locations. The results show that the time of maximum diurnal rainfall does not indicate robust seasonal variation, while the amplitude of diurnal rainfall indicates seasonal variation Figure 3. The time of maximum diurnal rainfall occurred between 2.00 and 4.00 PM, except for the OKI-2 station and SALEH-2 station, which were at 13.00 during the SON season and at 17.00 during the DJF season, respectively. In general, the time of maximum diurnal rainfall of the ECMWF-ERA5 data is faster than that of the SESAME station data. Meanwhile, the amplitude of diurnal rainfall during JJA and SON seasons is lower than that during DJF and MAM seasons.

The accuracy and uncertainty of ERA5 data when compared with in situ SESAME data which are considered to have actual data. it can be seen that the highest HIT occurs at MUBA-2 station, and the lowest is at MUBA-1. This is because there are quite a lot of data gaps in MUBA-1. The highest MISS occurred in OKI-2. False Highest alarm recorded on MUBA-2. The highest negative correction was recorded in Mud-2. Overall, due to data gaps that exist in the SESAME insitu data, there is a difference in the total number of all SESAME stations in the contingency table analysis.The details are shown in Table 6.

The bias score and CSI are shown in Table 7. The bias score from the ERA5 data shows that overall the ERA5 data underestimates the SESAME data. This is indicated by the value of False

 

**Table 4.** Percentage of completeness of the SESAME data (%)

| YEAR | MONTH | OKI-1 | OKI-2 | MUBA-1 | MUBA-2 | LUMPUR-1 | LUMPUR-2 | SALEH-1 | SALEH-2 |
|---|---|---|---|---|---|---|---|---|---|
| 2017 | JAN | 100 | 80 | 100 | 0 | 0 | 0 | 0 | 0 |
| 2017 | FEB | 100 | 60 | 65 | 59 | 0 | 0 | 0 | 0 |
| 2017 | MAR | 100 | 100 | 90 | 100 | 0 | 0 | 0 | 0 |
| 2017 | APR | 100 | 100 | 100 | 100 | 0 | 0 | 0 | 0 |
| 2017 | MAY | 100 | 100 | 100 | 100 | 0 | 0 | 0 | 0 |
| 2017 | JUN | 100 | 100 | 100 | 100 | 59 | 55 | 45 | 41 |
| 2017 | JUL | 100 | 100 | 100 | 100 | 100 | 100 | 100 | 100 |
| 2017 | AUG | 100 | 100 | 100 | 100 | 100 | 100 | 100 | 100 |
| 2017 | SEP | 100 | 100 | 94 | 100 | 100 | 100 | 100 | 100 |
| 2017 | OCT | 100 | 100 | 49 | 100 | 100 | 100 | 100 | 100 |
| 2017 | NOV | 100 | 100 | 61 | 100 | 100 | 100 | 100 | 100 |
| 2017 | DEC | 100 | 100 | 14 | 100 | 100 | 100 | 100 | 100 |
| 2018 | JAN | 100 | 100 | 0 | 99 | 100 | 100 | 100 | 100 |
| 2018 | FEB | 100 | 100 | 0 | 100 | 100 | 100 | 100 | 100 |
| 2018 | MAR | 100 | 100 | 0 | 100 | 100 | 100 | 100 | 100 |
| 2018 | APR | 100 | 100 | 0 | 100 | 100 | 100 | 100 | 100 |
| 2018 | MAY | 60 | 100 | 0 | 100 | 100 | 100 | 100 | 100 |
| 2018 | JUN | 81 | 100 | 0 | 100 | 100 | 100 | 100 | 100 |
| 2018 | JUL | 100 | 100 | 0 | 100 | 100 | 100 | 100 | 100 |
| 2018 | AUG | 100 | 100 | 0 | 100 | 100 | 100 | 100 | 100 |
| 2018 | SEP | 100 | 100 | 0 | 100 | 100 | 100 | 100 | 100 |
| 2018 | OCT | 100 | 100 | 0 | 100 | 100 | 100 | 100 | 100 |
| 2018 | NOV | 100 | 100 | 0 | 100 | 100 | 100 | 100 | 100 |
| 2018 | DEC | 100 | 18 | 0 | 100 | 100 | 100 | 100 | 100 |
| 2019 | JAN | 12 | 56 | 0 | 100 | 100 | 100 | 100 | 100 |
| 2019 | FEB | 0 | 100 | 0 | 98 | 100 | 97 | 100 | 100 |
| 2019 | MAR | 0 | 68 | 0 | 100 | 100 | 100 | 100 | 57 |
| 2019 | APR | 0 | 100 | 0 | 100 | 100 | 100 | 100 | 15 |
| 2019 | MAY | 0 | 99 | 0 | 60 | 90 | 90 | 83 | 1 |
| 2019 | JUN | 0 | 100 | 0 | 0 | 100 | 100 | 68 | 100 |
| 2019 | JUL | 0 | 25 | 0 | 0 | 100 | 100 | 100 | 100 |
| 2019 | AUG | 0 | 0 | 0 | 0 | 100 | 100 | 100 | 100 |
| 2019 | SEP | 0 | 0 | 0 | 0 | 100 | 57 | 100 | 100 |
| 2019 | OCT | 0 | 0 | 0 | 0 | 100 | 100 | 100 | 100 |
| 2019 | NOV | 0 | 0 | 0 | 0 | 100 | 100 | 100 | 100 |
| 2019 | DEC | 0 | 0 | 0 | 0 | 100 | 61 | 100 | 19 |

**Table 5.** The time of maximum diurnal rainfall observed at the SESAME stations during different season

| Station | DJF season | MAM season | JJA season | SON season |
|---|---|---|---|---|
| OKI-1 | 11:00 PM | 11:00 PM | 11:00 PM | 8:00 PM |
| OKI-2 | 11:00 PM | 8:00 PM | 11:00 PM | 11:00 PM |
| MUBA-1 | 11:00 PM | 11:00 PM | 11:00 PM | 11:00 PM |
| MUBA-2 | 11:00 PM | 11:00 PM | 11:00 PM | 11:00 PM |
| Lumpur-1 | 11:00 PM | 5:00 PM | 5:00 PM | 11:00 PM |
| Lumpur-2 | 8:00 PM | 5:00 PM | 11:00 PM | 11:00 PM |
| Seleh-1 | 10:00 PM | 11:00 PM | 11:00 PM | 11:00 PM |
| Seleh-2 | 11:00 PM | 11:00 PM | 5:00 PM | 5:00 PM |

**Table 6.** Result table contigency

| | HIT | MISS | FALSE ALARM | CORRECT NEGATIF | TOTAL | TOTAL ERROR |
|---|---|---|---|---|---|---|
| OKI-1 | 588 | 296 | 5109 | 296 | 6289 | 9102 |
| OKI-2 | 656 | 402 | 6053 | 402 | 7513 | 5825 |
| MUBA-1 | 216 | 116 | 2162 | 116 | 2610 | 19165 |
| MUBA-2 | 644 | 379 | 6547 | 379 | 7949 | 6466 |
| LUMPUR-1 | 610 | 338 | 5969 | 338 | 7255 | 3996 |
| LUMPUR-2 | 552 | 341 | 6223 | 341 | 7457 | 4377 |
| SELEH-1 | 618 | 329 | 5913 | 329 | 7189 | 4645 |
| SELEH-2 | 538 | 162 | 6210 | 162 | 7072 | 6309 |

**Table 7.** Table BIAS Score and Crittical Sucses Index (CSI)

| | BIASS | CSI |
|---|---|---|
| OKI-1 | 0.155169 | 0.098114 |
| OKI-2 | 0.157699 | 0.092251 |
| MUBA-1 | 0.139613 | 0.086608 |
| MUBA-2 | 0.142261 | 0.085073 |
| LUMPUR-1 | 0.144095 | 0.088189 |
| LUMPUR-2 | 0.131808 | 0.077572 |
| SELEH-1 | 0.145001 | 0.090087 |
| SELEH-2 | 0.103734 | 0.077858 |

Alarm which is higher than the value of the miss event from ERA5 data. Besides that, CSI also shows that ERA5 has not been able to model rainfall events at each location well enough. Thus the overall accuracy and uncertainty of ERA5 data in this case is hourly data, not being able to model rainfall events at each SESAME station location quite well.

### 3.2 Spatial variation of time of maximum diurnal rainfall

Spatial harmonic analysis has been performed on the ECMWF-ERA5 data to evaluate the spatial variation of the time of maximum diurnal rainfall (Figure 4). In general, the time of maximum diurnal rainfall did not show robust spatial variation. Over the ocean, the time of maximum diurnal rainfall occurs during night time/early morning (1:00 – 4:00 AM). Over the lowland or coastal area, the time of maximum diurnal rainfall occurs during the afternoon (14:00 – 16:00), while over the high altitude (mountain) it occurs during the late-night around 21:00 – 23:00 Close examination on the seasonal variation, there is a shift of the time of maximum diurnal rainfall over the eastern coast of Sumatera during the dry season (JJA and SON). The time of maximum rainfall during these seasons occurs in the early afternoon around 11:00 – 13:00.

## 4. CONCLUSIONS

Characteristics of diurnal rainfall over the peatland of South Sumatera was evaluated by using in situ data obtained from the SESAME project combined with the reanalysis data of the ECMWF-ERA5. A harmonic analysis was applied both on the single time series and the gridded (spatial) data to obtained the amplitude and phase of the diurnal signal.

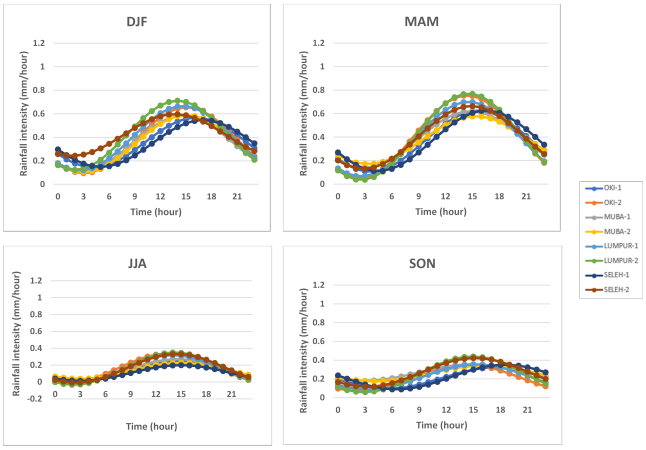


**Figure 3.** Same as Figure 2 except for the precipitation data obtained from the ECMWF-ERA5

The results show that the diurnal peak of rainfall over the study area mostly occurs during afternoon ranging from 17.00 to 23.00 Western Indonesian Time. Interestingly, the in situ data revealed seasonal variation both in amplitude and time of maximum diurnal rainfall. Minimum amplitude of diurnal rainfall was observed during the dry season (JJA), while high amplitude was observed during other seasons. Meanwhile, the reanalysis data only indicated a weak seasonal variation on the amplitude of the diurnal rainfall. Minimum amplitude of diurnal rainfall appears during JJA as well as SON seasons, while relatively high amplitude was observed in DJF and MAM seasons. Furthermore, spatial analysis shows that the time of maximum diurnal rainfall has spatial variation. Over the ocean, the time of maximum diurnal rainfall occurs during night time/early morning. Over the lowland or coastal area, the time of maximum diurnal rainfall occurs during afternoon, while over the high altitude (mountain) it occurs during late night.

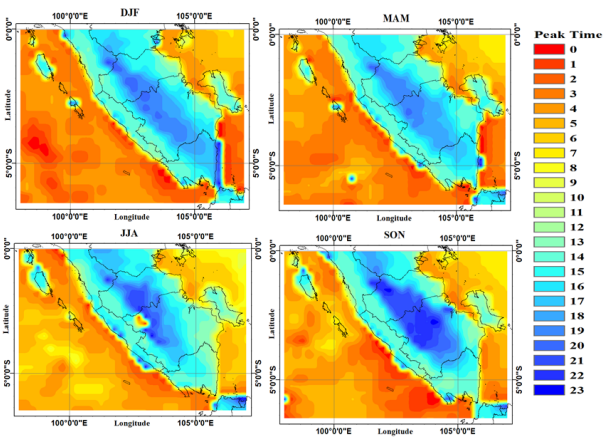


**Figure 4.** Spatial variations of time of maximum diurnal rainfall for DJF (top left), MAM (top right), JJA (bottom left), and SON (bottom right) seasons obtained from the ECMWF-ERA5 data.

## 5. ACKNOWLEDGEMENT

We thank to the Peatland Restoration Agency for providing us the SESAME data. This study is supported by the University of Sriwijaya through the Hibah Unggulan Profesi 2020 for the last author.

## REFERENCES

Angelis, C., G. McGregor, and C. Kidd (2004). Diurnal cycle of rainfall over the Brazilian Amazon. *Climate Research*, **26**; 139–149

Biasutti, M., S. E. Yuter, C. D. Burleyson, and A. H. Sobel (2011). Very high resolution rainfall patterns measured by TRMM precipitation radar: seasonal and diurnal cycles. *Climate Dynamics*, **39**(1-2); 239–258

Gray, W. M. and R. W. Jacobson Jr (1977). Diurnal variation of deep cumulus convection. *Monthly Weather Review*, **105**(9); 1171–1188

Houze Jr, R. A., S. G. Geotis, F. D. Marks Jr, and A. K. West (1981). Winter monsoon convection in the vicinity of north Borneo. Part I: Structure and time variation of the clouds and precipitation. *Monthly Weather Review*, **109**(8); 1595–1614

Mori, S., H. Jun-Ichi, Y. I. Tauhid, M. D. Yamanaka, N. Okamoto, F. Murata, N. Sakurai, H. Hashiguchi, and T. Sribimawati (2004). Diurnal land–sea rainfall peak migration over Sumatera Island, Indonesian Maritime Continent, observed by TRMM satellite and intensive rawinsonde soundings. *Monthly Weather Review*, **132**(8); 2021–2039

Murakami, M. (1983). Analysis of the Deep Convective Activity Over the Western Pacific and Southeast Asia. *Journal of the Meteorological Society of Japan. Ser. II*, **61**(1); 60–76

Putra, R. (2019). UNDERSTANDING OF FIRE DISTRIBUTION IN THE SOUTH SUMATRA PEAT AREA DURING THE LAST TWO DECADES. *International Journal of GEOMATE*, **16**(54)

Putra, R., D. O. Lestari, E. Sutriyono, S. Sabaruddin, and I. Iskandar (2019). Dynamical Link of Peat Fires in South Sumatra and the Climate Modes in the Indo-Pacific Region. *Indonesian Journal of Geography*, **51**(1); 18

Stull, R. B. et al. (2018). Practical meteorology: an algebra-based survey of atmospheric science

 